ISSN: 2710-0588

Molybdenum Ion Doping for Enhanced Performance of High-Nickel $LiNi_{0.8}Co_{0.1}Mn_{0.1}O_2$ Ternary Cathodess

Jun Gou*, Jingyang Hu, Qiang Xu, Qijun Ran

College of Mechanical Engineering, Sichuan University of Science & Engineering, Yibin, China

*Corresponding Author: Gou Jun

Abstract

To enhance the structural and chemical stability of $LiNi_{0.8}Co_{0.1}Mn_{0.1}O_2$ (NCM811), a series of Mo-doped NCM811 electrolytes (Mo_x-NCM811, x = 0-0.03) were synthesized via high-energy mechanical ball milling followed by high-temperature sintering. XRD phase analysis, GASA II refinement, and SEM characterization revealed that appropriate Mo doping effectively reduces the ion migration impedance, enhances Li^+ diffusion coefficient, and stabilizes the material structure, thereby improving both discharge specific capacity and cycling performance. When the Mo doping level reaches x=0.02, the optimized material demonstrates a first-cycle discharge capacity of 213.4 mAh/g at 0.1C rate and maintains 88.51% capacity retention after 100 cycles at 1C rate, significantly surpassing the undoped sample's 84% retention. Notably, the capacity retention remains at 89.4% even after multiple rate cycling tests (various rates for 5 cycles each) followed by returning to 0.1C rate.

Keywords

Lithium-ion batteries;$LiNi_{0.8}Co_{0.1}Mn_{0.1}O_2$;Mo doping; electrochemical performance.

1. Introduction

Lithium-ion batteries (LIBs) have been widely adopted in portable electronics and electric vehicles due to their high specific energy, cycling stability, and low environmental impact[1]–[4]. In recent years, to meet the escalating demand for energy density in electric vehicles, nickel-rich ternary cathode materials with the general formula $LiNi_xCo_yMn_{1-x-y}O_2$(NCM) have been developed[5]. Studies demonstrate that NCM cathodes with varying transition metal ratios, such as Ni:Co:Mn = 1:1:1 (NCM111)[6,7], 5:2:3 (NCM523)[8], 6:2:2 (NCM622)[9,10], and 8:1:1 (NCM811)[11], exhibit significantly enhanced energy density. Notably, NCM811 delivers a practical specific capacity of ≥200 mAh/g[11,12]. However, its layered structure is prone to transform into a rock-salt phase due to Ni^{2+} migration-induced structural instability. Additionally, Ni/Li cation mixing and poor thermal stability within the NCM811 lattice lead to severe performance degradation and safety concerns[13]-[15].

To address the structural instability of high-nickel ternary cathodes, substantial efforts have been devoted to doping strategies[13,16,17]. Heteroatom doping has been widely employed to stabilize the bulk and surface structure of cathodes, thereby enhancing electrochemical performance. Commonly used dopants include Al[18], Fe[19], Ti[20], Y[21], Nb[22], F[23] and Cl[24]. In this work, Mo doping is specifically selected owing to the higher bond dissociation energy of Mo-O (560 kJ/mol) compared to Ni-O (391.6 kJ/mol), Co-O (368 kJ/mol), and Mn-O (402 kJ/mol)[25]. The incorporation of Mo^{6+} into the NCM lattice is expected to suppress structural degradation and improve electrochemical performance[26,27].

In this study, Mo^{6+} ions with varying doping concentrations (0-3 mol%) were introduced into the NCM811 structure via high-temperature solid-state reaction using nano-sized MoO_3, co-precipitated $Ni_{0.8}Co_{0.1}Mn_{0.1}(OH)_2$ precursor, and $LiOH·H_2O$. Although doping strategies for

ISSN: 2710-0588

NCM811 cathodes have been extensively explored, only marginal improvements in electrochemical cycling performance have been achieved, and the underlying mechanisms remain ambiguous. Furthermore, limited research has focused on Mo^{6+}-doped NCM811 cathodes. A combination of characterization techniques, including XRD, SEM, and electrochemical testing systems, was employed to investigate the Mo^{6+}-doped NCM811 materials. The results reveal that Mo^{6+} doping significantly enhances the electrochemical performance of NCM cathodes, with an optimal doping concentration of 2 mol%.

2. Experiments

2.1. Material Preparation

The $LiNi_{0.8}Co_{0.1}Mn_{0.1}O_2$ cathode material was synthesized via a two-step high-temperature solid-state sintering process. Initially, a commercial $Ni_{0.8}Co_{0.1}Mn_{0.1}(OH)_2$ precursor and $LiOH{\cdot}H_2O$ lithium salt were homogeneously mixed in a molar ratio of 1:1.05. The mixture was first sintered at 500℃ under an oxygen atmosphere for 5 h, followed by a second sintering step at 780℃ for 10 h to yield the polycrystalline $LiNi_{0.8}Co_{0.1}Mn_{0.1}O_2$ cathode material.For the Mo-doped modified cathodes, stoichiometric amounts of the $Ni_{0.8}Co_{0.1}Mn_{0.1}(OH)_2$ precursor, $LiOH{\cdot}H_2O$, and MoO_3 (0.01 mol, 0.02 mol, and 0.03 mol, respectively) were uniformly blended. The resulting mixtures were subjected to identical sintering conditions (500 ℃ for 5 h and 780 ℃ for 10 h in oxygen) as the undoped material using a tube furnace.

2.2. Material Characterization

The phase structures of the samples were characterized by X-ray diffraction (XRD, Rigaku MiniFlex600) with Cu Kα radiation. Rietveld refinement analysis of the XRD data was performed using the GSAS II software. The morphology and elemental distribution of the samples were examined via scanning electron microscopy (SEM, JEOL JSM7500F) equipped with energy-dispersive X-ray spectroscopy (EDS).

2.3. Electrochemical performance testing

To assess the electrochemical properties, NCM811 and Mo-doped NCM811 samples were assembled into CR-2032 coin-type cells. The cathode materials were uniformly mixed with conductive agent (Super P) and binder (polyvinylidene fluoride, PVDF) at a mass ratio of 8:1:1. An appropriate amount of N-methyl-2-pyrrolidone (NMP) solvent was added to form a homogeneous slurry, which was then coated onto an aluminum foil current collector. The coated electrodes were dried in a convection oven at 120℃ for 12 hours to remove residual moisture, followed by punching into disks with an active material loading of ~4 mg/cm^2. The CR-2032 coin cells were assembled in an argon-filled glovebox, employing lithium metal as the counter/reference electrode, a Celgard 2300 separator, and an electrolyte containing 1 M $LiPF_6$ dissolved in a mixed solvent of ethylene carbonate (EC), dimethyl carbonate (DMC), and diethyl carbonate (DEC) (volume ratio 1:1:1).

Galvanostatic charge-discharge tests were conducted using a CT-4008 battery testing system (Neware Technology Co., Ltd.). Electrochemical impedance spectroscopy (EIS) measurements were performed on a CHI660E electrochemical workstation (CH Instruments, Shanghai) over a frequency range of 100 kHz to 10 mHz with an amplitude of 5 mV. The acquired data were subsequently fitted and analyzed using ZView impedance modeling software. The lithium-ion diffusion coefficient (D_{Li^+}) was calculated from the low-frequency region of the Nyquist plots, as expressed in Equation (2.1):

$$D_{Li}^{+} = \frac{R^2T^2}{2A^2n^4F^4C^2\sigma^2} \tag{2.1}$$

ISSN: 2710-0588

In Equation (2.1), R represents the gas constant (8.314 J K^{-1} mol^{-1}), T denotes the absolute temperature (298.15 K), n is the number of electrons transferred during the electrode reaction, A is the electrode surface area, F is the Faraday constant (96485 s A mol^{-1}), and σ corresponds to the Warburg factor.The Warburg factor (σ) can be calculated using Equation (2.2) :

$$Z' = Rsf + Rct + \sigma\omega^{-0.5} \quad (2.2)$$

In the above equations, Z' represents the real component of the impedance (resistive portion), Rsf denotes the interfacial film resistance, which includes contributions from the solid electrolyte interphase (SEI) and coating layer resistance, Rct is the charge transfer resistance,and ω corresponds to the low-frequency angular frequency. The values of these parameters can be directly extracted from the Nyquist plots and will be utilized for subsequent EIS analysis.

3. Results and Discussion

3.1. XRD profiling

In order to investigate the effects of different ratios of Mo^{6+} doping on the crystal structure and Li/Ni mixing degree of NCM811 cathode materials, they were characterised and analysed using XRD, and the results are shown in Figure 3-1.

Figure 3-1 shows the XRD patterns of NCM811, $Mo_{0.01}$-NCM811, $Mo_{0.02}$-NCM811 and $Mo_{0.03}$-NCM811. As shown in Figure 3-1, the cathode materials prepared with Mo-NCM811 at different molybdenum doping levels are all with α-$NaFeO_2$ hexagonal layered structure, R-3m space group, and the peak positions of several main diffraction peaks appearing at 2θ=18, 36, 38, 44, and 64° are in agreement with those of the standard card of LiNiO2 (PDF#74-0919). A careful observation of the XRD patterns in Fig. 3-5a shows that the XRD patterns of NCM811 cathode materials doped with different ratios of Mo6+ do not show any characteristic peaks about Mo or other impurity diffraction, which suggests that Mo is doped into the crystal lattice of NCM811 cathode materials in the form of Mo6+ and will not damage the crystal structure of NCM cathode materials[28]. As shown in Figure 3-5b, the shift of the (003) peak shows that the (003) peak is gradually shifted to the left with the increase of Mo addition, and the peak intensity decreases and the peak shape changes. The shift of the (003) diffraction peak to the left indicates that the interlayer spacing in the lattice becomes larger, and the decrease in peak intensity indicates that the orientation of the (003) crystal surface becomes weaker, and the change in the peak shape may be caused by grain refinement[29]. The (018)/(110) diffraction peaks of Mo-NCM811 cathode material are cleaved as shown in Fig. 3-5c, but with the increase of Mo doping, the (108)/(110) cleavage peaks are gradually overlapped, which indicates that the laminar structure is less and less obvious.The XRD results indicate that Mo doping into the lattice causes the lattice changes. In addition, the peak intensity ratios of (003)/(104) for the comparison sample NCM811, the doped sample $Mo_{0.01}$-NCM811, $Mo_{0.02}$-NCM811 and $Mo_{0.03}$-NCM811 cathode samples are 1.61, 1.58, 1.54 and 1.46, respectively, and the ratio of R gradually decreases, which suggests that the more Mo is added, the more serious Li/Ni mixing is. This indicates that the more Mo is added, the more serious Li/Ni mixing is, due to the fact that in order to balance the charge, the addition of high valence Mo^{6+} (ionic radius 0.62 Å) leads to the increase of Ni^{3+} (ionic radius 0.62 Å) reducing Ni^{2+} (ionic radius 0.72 Å) in the bulk phase of the material, which increases the spacing of the layers, and at the same time, the Ni^{2+} with a large ionic radius is easy to migrate to the Li layer, resulting in an increase of mixing and rearranging[30].

ISSN: 2710-0588

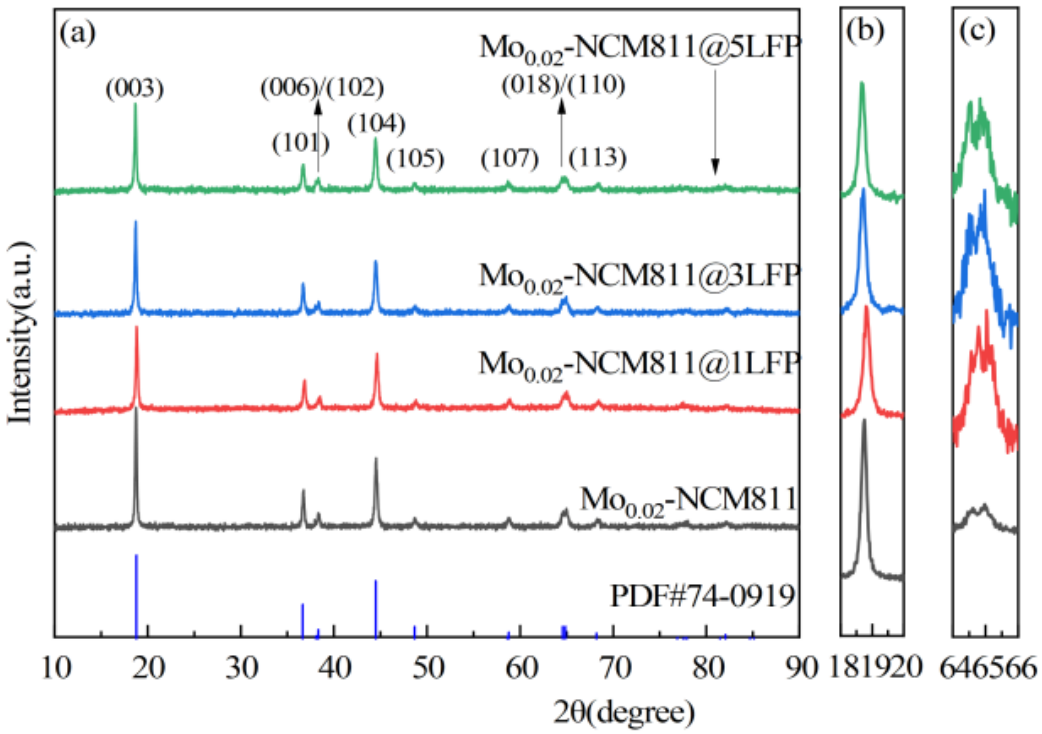

Figure 3-1. XRD patterns of NCM811, Mo0.01-NCM811, Mo0.02-NCM811 and Mo0.03-NCM811

(a)Overall XRD pattern; (b) (003) local magnification; (c) (108)/(110) cleavage peak magnification

In order to further determine the effect of Mo^{6+} doped NCM811 cathode material on the cell parameters, the XRD data were subjected to Rietveld refinement using GSAS software[31], and the results are shown in Fig. 3-2, and the corresponding data are listed in Table 3-1. From the fit, the fitting R-factor (Rp and Rwp are less than 10%), the confidence level is high. From the table, it can be seen that the Li/Ni mixing and rearranging degrees of the comparison samples NCM811, the coating amount $Mo_{0.01}$-NCM811, $Mo_{0.02}$-NCM811 and $Mo_{0.03}$-NCM811 anode material samples are 3.49%, 4.13%, 5.02% and 6.12%, respectively, which is in line with the variation of the (003)/(104) peak-to-peak intensity ratio. It is worth noting that the cell parameters a, c and cell volume V increase and then decrease, and the Mo0.02-NCM811 cathode material sample exhibits the largest layer spacing and cell volume. c-axis direction of the cell parameters is determined by the layer spacing of the TMO_6 octahedra and the LiO_6 octahedra, and this octahedral spacing is related to the bonding angles of the O_1-Li-O_2 and the O_1-TM-O_2, and a certain level of of doping is required to lead to a simultaneous increase in the layer spacing of the TMO_6 octahedra and LiO_6 octahedra, with the cell parameter c being the largest. With increasing doping ($Mo_{0.03}$-NCM811), the TMO_6 octahedra increase more, the interlayer spacing of LiO_6 octahedra increases less, and the cell parameter c and cell volume V decrease instead.

ISSN: 2710-0588

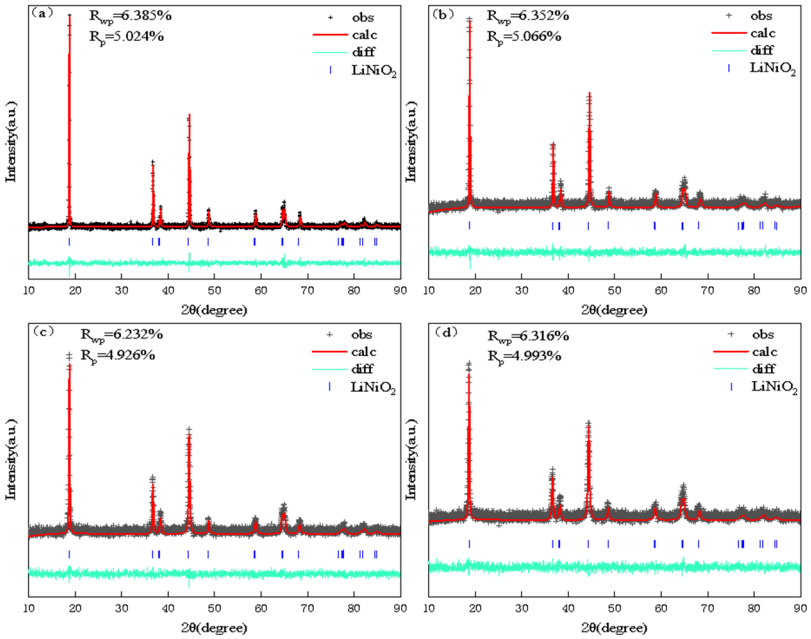

Figure 3-2. Finishing diagrams for NCM811、$Mo_{0.01}$-NCM811、$Mo_{0.02}$-NCM811 and $Mo_{0.03}$-NCM811

Table 3-1. Lattice parameters of $LiNi_{0.8}Co_{0.1}Mn_{0.1}O_2$samples prepared at different doping levels

Sample	a (Å)	c (Å)	V(Å^3)	c/a	R	Ni in Li site (%)
NCM811	2.87251	14.19219	101.41	4.94069	1.61	3.49
$Mo_{0.01}$-NCM811	2.87378	14.19361	101.51	4.939	1.58	4.13
$Mo_{0.02}$-NCM811	2.874245	14.20302	101.61	4.94148	1.54	5.02
$Mo_{0.03}$-NCM811	2.87453	14.19617	101.58	4.93861	1.46	6.12

3.2. SEM topography analysis

Figure 3-3 shows the SEM images of $LiNi_{0.8}Co_{0.1}Mn_{0.1}O_2$ with varying Mo doping levels. As illustrated in Figure 3-3(a, b), the undoped NCM811 exhibits a secondary spherical morphology composed of irregular primary particles with non-uniform sizes (approximately 10 μm in diameter), including some larger primary particles. Figures 3-3(c, d, e, f, g, h) display the SEM images of $Mo_{0.01}$-NCM811, $Mo_{0.02}$-NCM811, and $Mo_{0.03}$-NCM811. It is evident that as the Mo doping level increases, the size of the secondary spheres gradually decreases, and the primary particles become more refined. This refinement likely reduces interparticle gaps, thereby inhibiting electrolyte penetration and enhancing the electrochemical performance of the NCM811 cathode material[32].For $Mo_{0.02}$-NCM811, the primary particles within the secondary spheres are significantly smaller and more uniform in size compared to those of undoped NCM811, which is advantageous for improving chemical stability. However, compared to $Mo_{0.02}$-NCM811, $Mo_{0.01}$-NCM811 shows smaller primary particles with insufficiently developed morphology and more pronounced gaps. In contrast, $Mo_{0.03}$-NCM811 exhibits agglomeration of primary particles and compromised integrity of the secondary spheres, including partial

ISSN: 2710-0588

surface collapse and adhesion of fine particles, resulting in blurred boundaries. This phenomenon may arise from excessive Mo doping, where residual Mo-containing compounds (unable to enter the crystal lattice due to solubility saturation) accumulate on particle surfaces, forming poorly conductive phases[33]. These surface phases act similarly to a coating layer, which could detrimentally affect the electrochemical performance of the cathode material.

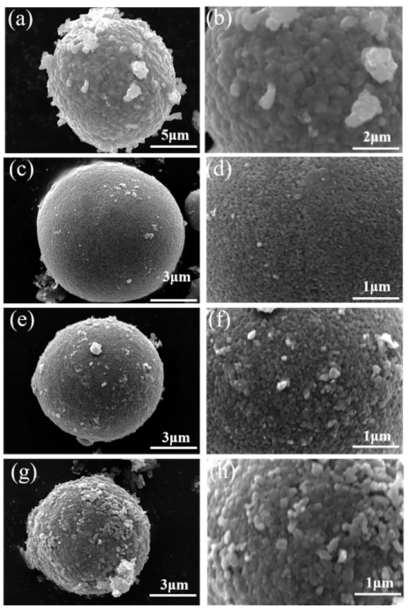

Figure 3-3. SEM images of $LiNi_{0.8}Co_{0.1}Mn_{0.1}O_2$ prepared with varying Mo doping levels [(a) and (b) show the overall view and locally magnified view of the NCM811 sample, respectively; (c) and (d) correspond to the $Mo_{0.01}$-NCM811 sample; (e) and (f) and (g) and (h) display the overall and magnified views of the $Mo_{0.02}$-NCM811 and $Mo_{0.03}$-NCM811 samples, respectively.]

The elemental distributions of Ni, Co, Mn, and Mo in the NCM811 and $Mo_{0.02}$-NCM811 cathode materials were characterized via energy-dispersive X-ray spectroscopy (EDS), as demonstrated in the EDS-mapping images (Fig. 3-4).

As shown in Figs. 3-4a and 3-4b, Ni, Co, and Mn exhibit homogeneous spatial dispersion across both the pristine NCM811 and Mo-modified $Mo_{0.02}$-NCM811 particles. Notably, Mo was exclusively detected in the $Mo_{0.02}$-NCM811 sample, with its elemental mapping regions highly overlapping with those of Ni, Co, and Mn. This observation confirms the successful incorporation of Mo^{6+} ions into the bulk lattice of NCM811, consistent with substitutional doping at transition metal sites.

As shown in Figs. 3-4a and 3-4b, Ni, Co, and Mn exhibit homogeneous spatial dispersion across both the pristine NCM811 and Mo-modified $Mo_{0.02}$-NCM811 particles. Notably, Mo was exclusively detected in the $Mo_{0.02}$-NCM811 sample, with its elemental mapping regions highly overlapping with those of Ni, Co, and Mn. This observation confirms the successful incorporation of Mo^{6+} ions into the bulk lattice of NCM811, consistent with substitutional doping at transition metal sites.

ISSN: 2710-0588

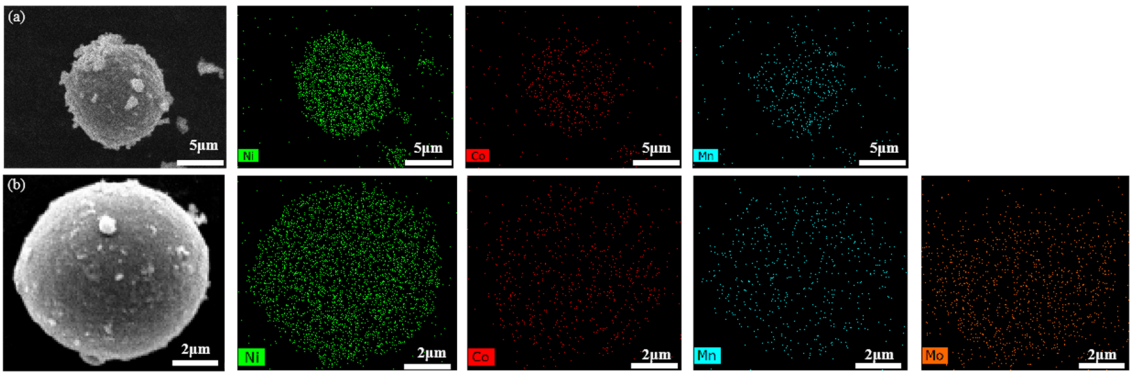

Figure 3-4. EDS elemental mapping images: (a)NCM811，(b)$Mo_{0.02}$-NCM811

Subsequently, the NCM811 and $Mo_{0.02}$-NCM811 materials were tested by ICP-OES, and the elemental components are listed in Table 3-2. According to the data analysis, the content ratio of Ni, Co and Mn in $Mo_{0.02}$-NCM811 material is close to 8:1:1, and the content of Mo element is close to 2%, which is in line with the stoichiometric ratio of $Mo_{0.02}$-NCM811 material experimental design.

Table 3-2. Elemental components of NCM811 and $Mo_{0.02}$-NCM811 cathode materials

Sample	Ingredients (%)			
	Ni	Co	Mn	Mo
NCM811	81.1	9.84	10.2	--
$Mo_{0.02}$-NCM811	80.3	10	9.4	1.8

3.3. Electrochemical analysis

In order to explore the effects of different proportions of Mo^{6+} doping on the electrochemical properties of NCM811 cathode material, the first charge-discharge, cycling performance and rate performance were carried out, and the test results are shown in Figs. 3-5, Fig. 3-6 and Fig. 3-7.

All samples were electrochemically studied to check the electrochemical properties of the Mo-doped NCM811 cathode material. Figure 3-5 shows the first cycle charge-discharge curve of a sample with different Mo doping amounts at 0.1C magnification. As shown in Figure 3-5, the initial current-static charge-discharge curves for each cathode material at room temperature with a voltage window of 2.8-4.3 V and 0.1 C. According to the electrochemical behavior of the doped material, the Mo-doped cathode material exhibits the original charge-discharge plateau at around 3.8 V, and no additional plateau appears, indicating that the electrochemical reaction of the doped NCM811 has not changed. The initial discharge capacitances of the comparison NCM, doped samples $Mo_{0.01}$-NCM811, $Mo_{0.02}$-NCM811 and $Mo_{0.03}$-NCM811 cathode materials were 192.8, 207.7, 213.4 and 200.9 mAh/g, respectively, and the corresponding Coulombic efficiencies (CEs) were 89.67%, 89.71%, 89.96% and 89.68%, respectively. Among them, the Mo0.02-NCM811 sample showed the best discharge specific capacity. From the perspective of unit cell parameters, the amount of Mo doping in a certain amount is conducive to increasing the spacing of lithium layers and the diffusion of lithium ions, while the doping amount is too high and causes the spacing of lithium layers to decrease, so the discharge specific capacity of $Mo_{0.02}$-NCM811 sample is the highest.

ISSN: 2710-0588

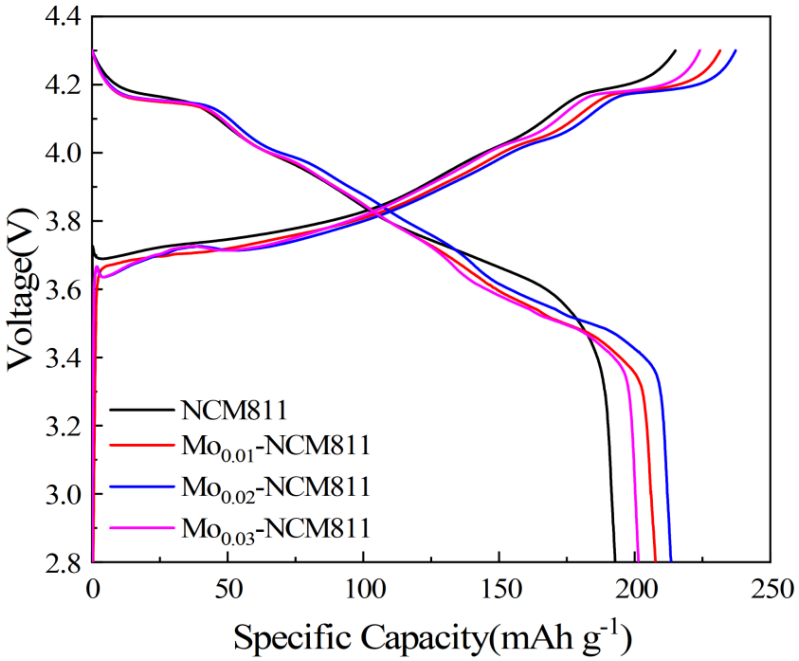

Figure 3-5. Charge-discharge curves of samples with different molybdenum doping amounts at 0.1C magnification

Figure 3-6 shows the 1C rate cycle diagram of the samples with different Mo doping amounts, as shown in Figure 3-14, the comparison sample NCM, the doped sample $Mo_{0.01}$-NCM811, $Mo_{0.02}$-NCM811, and the $Mo_{0.03}$-NCM811 cathode material samples after 100 cycles were 133.9, 145.3, 155.7, and 140.3 mAh/g, respectively, and the capacity retention rates were 84%, 86.38%, and 88.51%, respectively and 85.28%. With the increase of Mo doping, the structure of the material is more stable and the capacity is better maintained, and the best doping sample is $Mo_{0.02}$-NCM811. From the perspective of unit cell parameters, a certain amount of Mo doping is conducive to expanding the lithium layer spacing and lithium ion diffusion, while when the Mo doping amount is too high ($Mo_{0.03}$-NCM811), the lithium layer spacing decreases, so the discharge specific capacity of $Mo_{0.02}$-NCM811 sample is the highest.

Figure 3-6 shows the 1C rate cycle diagram of the samples with different Mo doping amounts, as shown in Figure 3-14, the comparison sample NCM, the doped sample $Mo_{0.01}$-NCM811, $Mo_{0.02}$-NCM811, and the $Mo_{0.03}$-NCM811 cathode material samples after 100 cycles were 133.9, 145.3, 155.7, and 140.3 mAh/g, respectively, and the capacity retention rates were 84%, 86.38%, and 88.51%, respectively and 85.28%. With the increase of Mo doping, the structure of the material is more stable and the capacity is better maintained, and the best doping sample is $Mo_{0.02}$-NCM811. From the perspective of unit cell parameters, a certain amount of Mo doping is conducive to expanding the lithium layer spacing and lithium ion diffusion, while when the Mo doping amount is too high ($Mo_{0.03}$-NCM811), the lithium layer spacing decreases, so the discharge specific capacity of $Mo_{0.02}$-NCM811 sample is the highest.

ISSN: 2710-0588

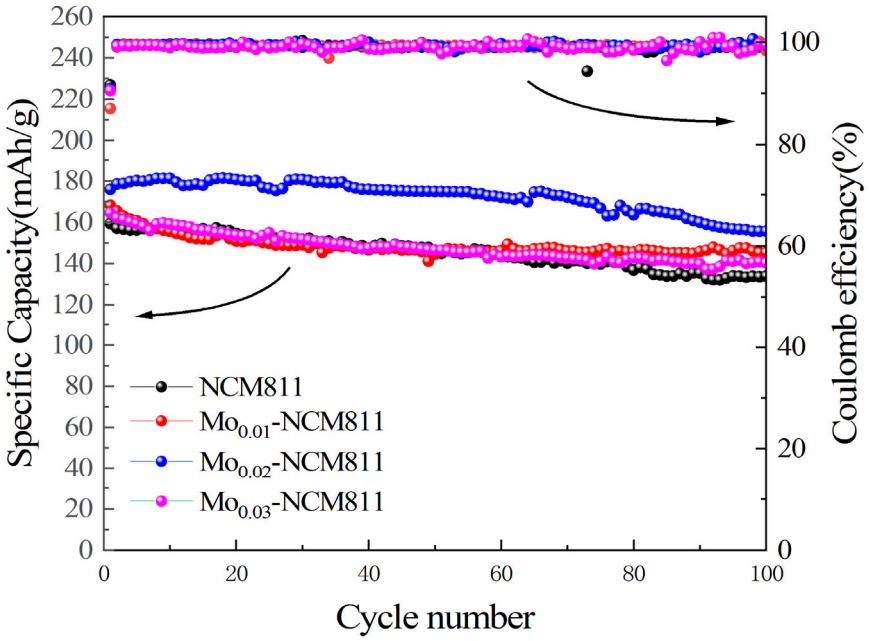

Figure 3-6. Cycling diagram of samples with different Mo doping amounts at 1C magnification

Figure 3-7 shows the performance of NCM811 samples with different Mo doping amounts at different C magnifications. The rate performance of the comparison sample NCM, doped sample $Mo_{0.01}$-NCM811, $Mo_{0.02}$-NCM811 and $Mo_{0.03}$-NCM811 cathode material samples at 0.1 C, 0.2 C, 0.5 C, 1 C, 2C and 5 C current densities was compared. As shown in Figure 3-7, the 5C discharge specific capacities of the comparison NCM, doped samples of $Mo_{0.01}$-NCM811, $Mo_{0.02}$-NCM811, and $Mo_{0.03}$-NCM811 are 120.5, 137.4, 150.9, and 132.5 mAh/g, respectively. The large-rate discharge specific capacity of the material is consistent with the change of 0.1C discharge specific capacity. In addition to the expansion of the spacing of lithium layers, the radial arrangement of primary particles in Mo-doped materials reduces the diffusion path of lithium ions, improves the consistency of charge transport, and improves the transport capacity of lithium ions. In the high delithiumation state, the crystal structure of the material is more likely to collapse, and the doping of Mo is conducive to maintaining the skeleton structure and lithium ion transport channel.

Table 3-3. Rate performance data of NCM and Mo-NCM cathode materials

Sample	0.1C (mAh/g)	0.2C (mAh/g)	0.5C (mAh/g)	1C (mAh/g)	2C (mAh/g)	5C (mAh/g)	0.1C (mAh/g)
NCM	192.8	185.6	174.6	159.4	148.6	120.5	164.3
$Mo_{0.01}$-NCM811	207.7	195.5	184.1	168.2	154.8	137.4	180.7
$Mo_{0.02}$-NCM811	213.4	204.7	188.8	175.9	168.4	150.9	190.8
$Mo_{0.03}$-NCM811	200.9	190.7	180.7	164.5	151.3	132.5	174.4

ISSN: 2710-0588

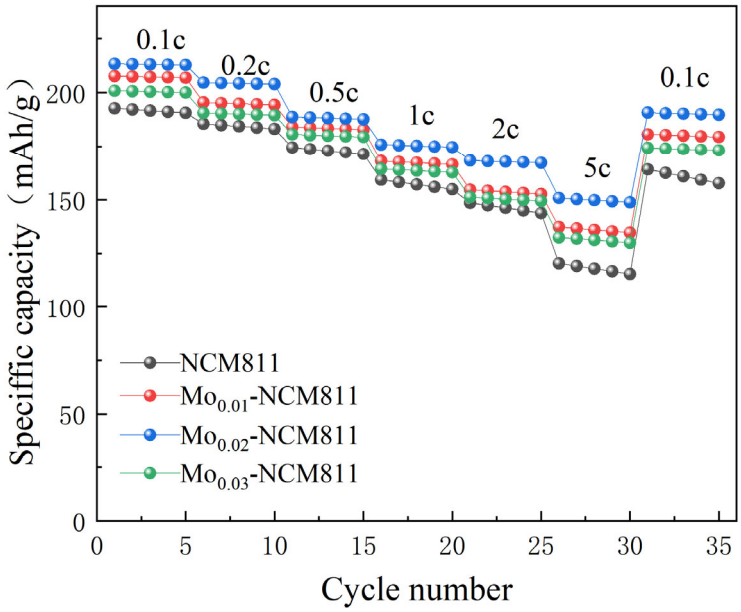

Figure 3-7. Performance of NCM811 samples with different Mo doping levels at different C magnifications

In order to explore the effects of different proportions of Mo^{6+} doping on the electrochemical reaction kinetics and reversibility of NCM811 cathode materials, cyclic voltammetry curves were carried out on NCM811 and Mo-NCM811 cathode materials, and the test results are shown in Figure 3-8.

Figure 3-8 shows the CV curves of NCM811 samples with different Mo doping amounts. As shown in Figure 3-16, there are three pairs of redox peaks in the CV curves of the comparison sample NCM, doped sample $Mo_{0.01}$-NCM811, $Mo_{0.02}$-NCM811, and $Mo_{0.03}$-NCM811 cathode material samples in the CV curve range of 3.45-3.97 V, 3.82-4.14 V, and 4.03-4.30 V. The redox peaks in the 3.45-3.97 V voltage range correspond to the oxidation and reduction reactions between Ni2+/Ni3+ and Ni^{4+} during the deintercalation of lithium ions, and the magnitude of the potential difference between the oxidation peaks and the reduction peaks, ΔV, can reflect the reversibility and polarization of the electrode reactions [34]. The potentials of the oxidation and reduction peaks of the comparison NCM, doped samples of $Mo_{0.01}$-NCM811, $Mo_{0.02}$-NCM811 and $Mo_{0.03}$-NCM811 were 3.84 V/3.69 V, 3.75 V/3.63 V, 3.74 V/3.64 V and 3.78 V/3.64 V, respectively, and the potential difference ΔV was 0.15 V, 0.12 V, 0.1 V and 0.14 V, respectively. Compared with the comparison sample, the potential difference ΔV of the doped samples $Mo_{0.01}$-NCM811, $Mo_{0.02}$-NCM811 and $Mo_{0.03}$-NCM811 decreased by 0.03V, 0.05V and 0.01V, respectively, and the potential difference decreased, and the potential difference of $Mo_{0.02}$-NCM811 was larger and more obvious. This indicates that the polarization degree of the electrode is reduced after Mo^{6+} doping with NCM811, which improves the reversibility during the electrochemical reaction, which is conducive to the redox reaction and the embedding and removal of Li^{+} during the charge-discharge process. Compared with other samples with Mo^{6+} doping, the potential difference of $Mo_{0.02}$-NCM811 is small, which corresponds to the results of significantly improved rate performance and cycling performance.

ISSN: 2710-0588

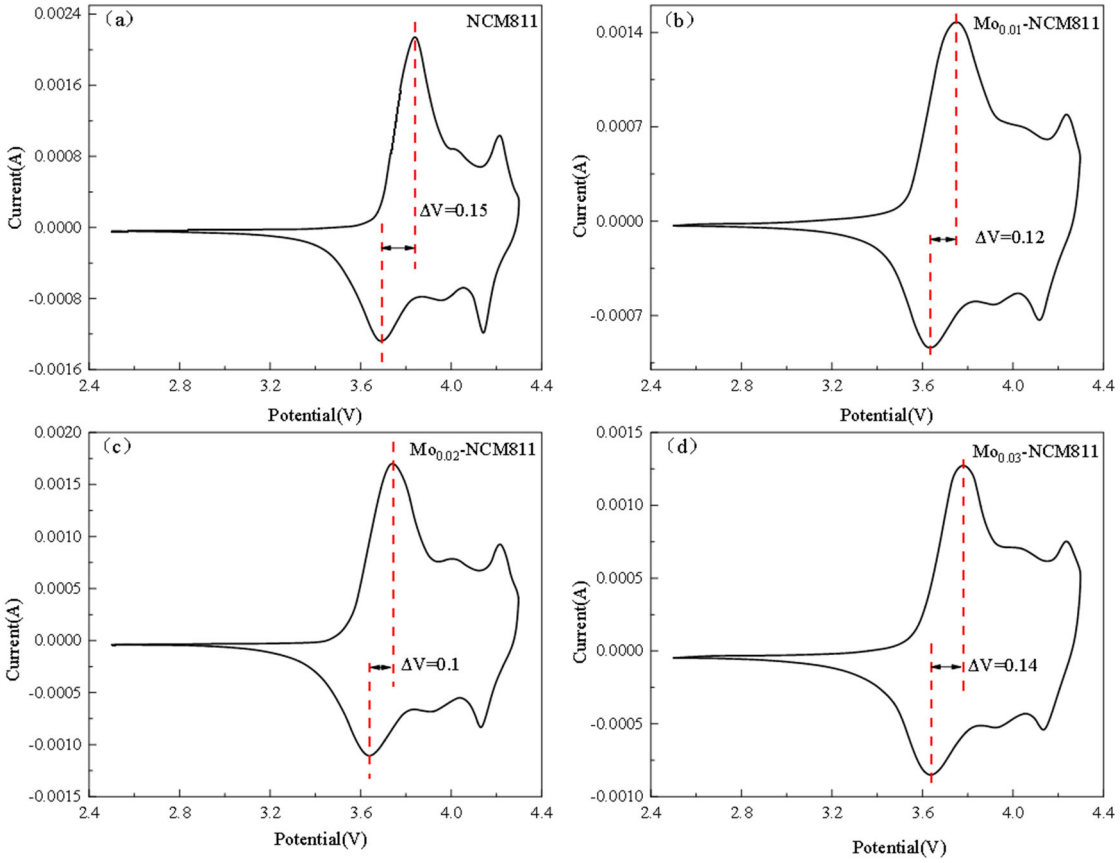

Figure 3-8. shows the CV curves of NCM811 samples with different Mo doping amounts

The AC impedance of the Mo-NCM811 cathode material was tested to further explore the effect of Mo^{6+} doping on the reaction of the NCM811 electrode. Figure 3-9 shows the EIS spectra of the NCM and $Mo_{0.02}$-NCM811 cathode materials charged to 4.3 V before cycling. Fig. 3-9a is the Nyqusit diagram of NCM811 and Mo0.02-NCM811 cathode materials before cycling, and Fig. 3-9b is the $Z' \sim \omega^{-0.5}$ fitting diagram. The corresponding data are listed in Table 3-4.

As shown in Figure 3-9, the Nyqusit diagram consists of two semicircles in the high and mid-frequency regions and a straight line in the low frequency region. where the intercept on the real axis is the bulk resistance (Rs); The high-frequency region corresponds to the interfacial film resistance (Rsf), including the solid electrolyte interface resistance and the coating resistance. The mid-frequency region corresponds to the charge transfer resistance (Rct); The slope of the low frequencies corresponds to the Warburg impedance (Zω) [35,36]. The Rsol of the two samples is not very different because the same electrolyte is used, and the conductivity of the electrolyte does not change with the EIS test. As can be seen from Figures 4-11a and 4-11b and Table 4-4, the Rsf and Rct of NCM811 and $Mo_{0.02}$-NCM811 cathode materials are 63.1/208.7 and 47.75/129.74 Ω, respectively. The Rsf and Rct of $Mo_{0.02}$-NCM811 are smaller than those of NCM811, which may be due to the fact that Mo^{6+} doping increases the layer spacing of NCM811 cathode material and provides more Li^+ transport channels, which in turn improves the deintercalation ability of Li^+ and leads to faster electrode process kinetics. The lithium-ion diffusion coefficient can be calculated from equations (1.3) and (2.4), as shown in Table 4-4, with D_{Li^+} of 6.32×10^{-15} and 9.38×10^{-15}, respectively. It can be seen that the lithium-ion diffusion coefficient of the material is increased by NCM811 after Mo^{6+} doping, which is consistent with the results that the rate performance of the material is improved after Mo^{6+} doping with NCM811 cathode material.

ISSN: 2710-0588

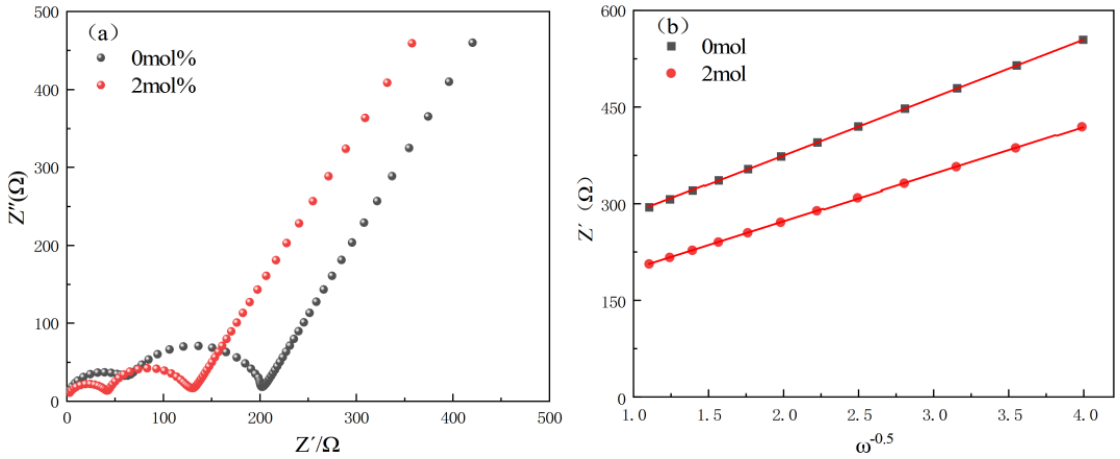

Figure 3-9. EIS spectra of NCM and $Mo_{0.02}$-NCM811 cathode materials charged to 4.3 V before cycling

(a) AC impedance diagram (b) $Z' \sim \omega^{-0.5}$ fitting diagram

Table 3-4. Impedance parameters and calculations of different proportions of Mo-doped NCM811 cathode materials D_{Li^+}

Sample	$R_s(\Omega)$	$R_{sf}(\Omega)$	$R_{ct}(\Omega)$	D_{Li^+}
NCM	3.37	63.1	208.7	6.32×10^{-15}
$Mo_{0.02}$-NCM811	3	47.75	129.74	9.38×10^{-15}

4. Summary

4.1. Summary

To investigate the impact of Mo doping levels on the electrochemical performance of Ni-rich $LiNi_{0.8}Co_{0.1}Mn_{0.1}O_2$(NCM811) cathode materials, this study synthesized Mo-doped NCM811 samples with varying Mo concentrations (0.01-0.03 mol) via high-energy mechanical ball milling combined with high-temperature sintering. Comprehensive characterization and analysis revealed that Mo doping enhances Li^+ diffusion kinetics, reduces polarization during charge/discharge, and improves cycling stability and Coulombic efficiency. However, excessive Mo incorporation exacerbated Li/Ni cation mixing, which became more pronounced at higher doping levels.The optimized 2 mol% Mo-doped sample ($Mo_{0.02}$-NCM811) exhibited balanced electrochemical performance, achieving a discharge capacity of 213.4 mAh/g at 0.1 C and a capacity retention of 88.51% after 100 cycles at 1 C. The pillar effect of Mo in the lithium layer and expanded interlayer spacing contributed to an elevated Li^+ diffusion coefficient ($9.38\times10^{-15}cm^2/s$) and a retained specific capacity of 150.9 mAh/g at 5 C, outperforming other samples. These results demonstrate that 2 mol% Mo doping optimally enhances the structural stability and rate capability of Ni-rich NCM811 while mitigating adverse cation disordering.

4.2. Hasdfhask

5. CONFLICTS OF INTEREST

The authors declare that they have no conflict of interest.

ISSN: 2710-0588

Acknowledgements

This work is supported by Research Project of Sichuan University of Science & Engineering Students Innovation and Entrepreneurship Training Program Project, Project Number: CX2023059

References

[1] Li H, Wang Z, Chen L, et al. Research on advanced materials for Li-ion batteries[J]. Advanced materials, 2009, 21(45): 4593-4607.

[2] Nitta N, Wu F, Lee J T, et al. Li-ion battery materials: present and future[J]. Materials today, 2015, 18(5): 252-264.

[3] Armand M, Tarascon J M. Building better batteries[J]. nature, 2008, 451(7179): 652-657.

[4] Tarascon J M, Armand M. Issues and challenges facing rechargeable lithium batteries[J]. nature, 2001, 414(6861): 359-367.

[5] Wang H, Sun D, Li X, et al. Alternative multifunctional cyclic organosilicon as an efficient electrolyte additive for high performance lithium-ion batteries[J]. Electrochimica Acta, 2017, 254: 112-122.

[6] Kasnatscheew J, Evertz M, Streipert B, et al. Changing established belief on capacity fade mechanisms: thorough investigation of LiNi1/3Co1/3Mn1/3O2 (NCM111) under high voltage conditions[J]. The Journal of Physical Chemistry C, 2017, 121(3): 1521-1529.

[7] Ohzuku T, Makimura Y. Layered lithium insertion material of LiNi1/3Co1/3Mn1/3O2 for lithium-ion batteries[J]. Chemistry letters, 2001, 30(7): 642-643.

[8] Shi Y, Zhang M, Qian D, et al. Ultrathin Al2O3 coatings for improved cycling performance and thermal stability of LiNi0.5Co0.2Mn0.3O2 cathode material[J]. Electrochimica Acta, 2016, 203: 154-161.

[9] Tao F, Yan X, Liu J J, et al. Effects of PVP-assisted Co3O4 coating on the electrochemical and storage properties of LiNi0.6Co0.2Mn0.2O2 at high cut-off voltage[J]. Electrochimica Acta, 2016, 210: 548-556.

[10] Deng B, Wang H, Ge W, et al. Investigating the influence of high temperatures on the cycling stability of a LiNi0.6Co0.2Mn0.2O2 cathode using an innovative electrolyte additive[J]. Electrochimica Acta, 2017, 236: 61-71.

[11] Kondrakov A O, Schmidt A, Xu J, et al. Anisotropic lattice strain and mechanical degradation of high- and low-nickel NCM cathode materials for Li-ion batteries[J]. The journal of physical chemistry C, 2017, 121(6): 3286-3294.

[12] Gong J, Wang Q, Sun J. Thermal analysis of nickel cobalt lithium manganese with varying nickel content used for lithium ion batteries[J]. Thermochimica acta, 2017, 655: 176-180.

[13] Sun H, Zhang Y, Li W, et al. Effects of Ag coating on the structural and electrochemical properties of LiNi0.8Co0.1Mn0.1O2 as cathode material for lithium ion batteries[J]. Electrochimica acta, 2019, 327: 135054.

[14] Lan G, Xing L, Bedrov D, et al. Enhanced cyclic stability of Ni-rich lithium ion battery with electrolyte film-forming additive[J]. Journal of alloys and compounds, 2020, 821: 153236.

[15] Lan G, Xing L, Bedrov D, et al. Enhanced cyclic stability of Ni-rich lithium ion battery with electrolyte film-forming additive[J]. Journal of alloys and compounds, 2020, 821: 153236.

[16] Schipper F, Bouzaglo H, Dixit M, et al. From surface ZrO2 coating to bulk Zr doping by high temperature annealing of nickel-rich lithiated oxides and their enhanced electrochemical performance in lithium ion batteries[J]. Advanced Energy Materials, 2018, 8(4): 1701682.

[17] Nanthagopal M, Santhoshkumar P, Shaji N, et al. Nitrogen-doped carbon-coated Li[Ni0.8Co0.1Mn0.1]O2 cathode material for enhanced lithium-ion storage[J]. Applied Surface Science, 2019, 492: 871-878.

[18] Do S J, Santhoshkumar P, Kang S H, et al. Al-doped Li [Ni0.78Co0.1Mn0.1Al0.02]O2 for high performance of lithium ion batteries[J]. Ceramics International, 2019, 45(6): 6972-6977.

ISSN: 2710-0588

[19] Wilcox J, Patoux S, Doeff M. Structure and electrochemistry of LiNi1⁄3Co1⁄3−yMyMn1⁄3O2 (M= Ti, Al, Fe) positive electrode materials[J]. journal of the electrochemical society, 2009, 156(3): A192.

[20] Zhang D, Liu Y, Wu L, et al. Effect of Ti ion doping on electrochemical performance of Ni-rich LiNi0.8Co0.1Mn0.1O2 cathode material[J]. Electrochimica acta, 2019, 328: 135086.

[21] Zhang M, Zhao H, Tan M, et al. Yttrium modified Ni-rich LiNi0.8Co0.1Mn0.1O2 with enhanced electrochemical performance as high energy density cathode material at 4.5 V high voltage[J]. Journal of Alloys and Compounds, 2019, 774: 82-92.

[22] Lv C, Yang J, Peng Y, et al. 1D Nb-doped LiNi1/3Co1/3Mn1/3O2 nanostructures as excellent cathodes for Li-ion battery[J]. Electrochimica Acta, 2019, 297: 258-266.

[23] Shin H S, Shin D, Sun Y K. Improvement of electrochemical properties of Li[Ni0.4Co0.2Mn(0.4-x)Mgx]O2-yFy cathode materials at high voltage region[J]. Electrochimica acta, 2006, 52(4): 1477-1482.

[24] Zhang H L, Wu F J. Effect of Cl doping on the structural and electrochemical properties of LiNi0.4Co0.2Mn0.4O2 as cathode materials for Lithium-ion Batteries[J]. International Journal of Electrochemical Science, 2020, 15(8): 7417-7422.

[25] Wang D, Li X, Wang Z, et al. Role of zirconium dopant on the structure and high voltage electrochemical performances of LiNi0.5Co0.2Mn0.3O2 cathode materials for lithium ion batteries[J]. Electrochimica Acta, 2016, 188: 48-56.

[26] Kaneda H, Koshika Y, Nakamura T, et al. Improving the cycling performance and thermal stability of LiNi0.6Co0.2Mn0.2O2 cathode materials by Nb-doping and surface modification[J]. International Journal of Electrochemical Science, 2017, 12(6): 4640-4653.

[27] Yang Z, Xiang W, Wu Z, et al. Effect of niobium doping on the structure and electrochemical performance of LiNi0.5Co0.2Mn0.3O2 cathode materials for lithium ion batteries[J]. Ceramics International, 2017, 43(4): 3866-3872.

[28] Shang G, Tang Y, Lai Y, et al. Enhancing structural stability unto 4.5 V of Ni-rich cathodes by tungsten-doping for lithium storage[J]. Journal of Power Sources, 2019, 423: 246-254.

[29] Sattar T, Lee S H, Jin B S, et al. Influence of Mo addition on the structural and electrochemical performance of Ni-rich cathode material for lithium-ion batteries[J]. Scientific Reports, 2020, 10(1): 8562.

[30] Aishova A, Park G T, Yoon C S, et al. Cobalt-free high-capacity Ni-rich layered Li[Ni0.9Mn0.1]O2 cathode[J]. Advanced energy materials, 2020, 10(4): 1903179.

[31] Ibrahim Al-jawfi, ZHAO Jiaqi, SHI Meng, et al. Cycling stability of Al-doped lithium manganese oxide materials in aqueous lithium-ion batteries [J]. Energy Storage Science and Technology, 2021, 10(04): 1330-1337.

[32] Sun H H, Kim U H, Park J H, et al. Transition metal-doped Ni-rich layered cathode materials for durable Li-ion batteries[J]. Nature communications, 2021, 12(1): 6552.

[33] KONG Dehao, LI Wei, TEGUS, et al. Preparation and modification of high-nickel ternary cathode material LiNi0.9Co0.05Mn0.05O2 for lithium-ion batteries [J]. Guangdong Chemical Industry, 2023, 50(18): 4-7+14.

[34] ZENG Zeng. Preparation and Modification of High-Nickel Ternary Cathode Materials [D]. Chengdu University, 2024. DOI:10.27917/d.cnki.gcxdy.2024.000496.

[35] Xiaoya Wang, Hao H , Liu J ,et al.A novel method for preparation of macroposous lithium nickel manganese oxygen as cathode material for lithium ion batteries [J]. Electrochimica Acta, 2011. DOI:10.1016/j.electacta.2010.12.108.

[36] Chen Y , Li P , Li Y ,et al.Enhancing the high-voltage electrochemical performance of the LiNi0.5Co0.2Mn0.3O2 cathode materials via hydrothermal lithiation[J].Journal of Materials ence, 2018.DOI:10.1007/s10853-017-1645-x.